Spatial modulation of second-harmonic generation via nonlinear Raman–Nath diffraction in an aperiodically poled lithium tantalite

Yuping Chen,[1,3] Weirui Dang,[1] Yuanlin Zheng,[1] Xianfeng Chen,[1,4] and Xuewei Deng[2]

[1]*State Key Laboratory on Fiber Optic Local Area Communication Networks and Advanced Optical Communication Systems, Department of Physics and Astronomy, Shanghai Jiao Tong University, 800 Dongchuan Rd., Shanghai 200240, China*

[2]*Laser Fusion Research Center, China Academy of Engineering Physics, Mianyang, Sichuan 621900, China*

[3]*e-mail: ypchen@sjtu.edu.cn*

[4]*e-mail: xfchen@sjtu.edu.cn*

Received April 3, 2013; revised May 22, 2013; accepted May 22, 2013;
posted May 23, 2013 (Doc. ID 188247); published June 26, 2013

We propose and experimentally demonstrate a colorful nonlinear Raman–Nath second-harmonic generation by engineering the quadratic nonlinearity $\chi^{(2)}$ in an aperiodically poled lithium tantalite. The engineered nonlinear structure allows multicolored Raman–Nath second-harmonic signal outputs along a uniform direction, which cannot be achieved in a uniform nonlinear grating. The diffraction angles are independent of the beam waist and the position of incidence. This verifies that nonlinear Raman–Nath diffraction does not depend on the local superlattice structure where the fundamental frequency beam locates, but on the whole nonlinear $\chi^{(2)}$ crystal. © 2013 Optical Society of America

OCIS codes: (190.4420) Nonlinear optics, transverse effects in; (190.2620) Harmonic generation and mixing; (050.1940) Diffraction.

http://dx.doi.org/10.1364/OL.38.002298

Second-harmonic generation (SHG), a versatile technique for creating coherent light at shorter wavelengths, has motivated great interest in physical study and applications over the past few decades. Usually, efficient quasi-phase-matching (QPM) SHG is realized by collinearly propagating the fundamental frequency (FF) and the second-harmonic (SH) beams along the QPM grating vector in periodic grating of the second-order $\chi^{(2)}$ nonlinearity, where only longitudinal phase matching takes place [1–4]. When the FF beam is noncollinear with the QPM grating vector, a transversely phase-matched nonlinear process [5–8] is introduced and the SH beam diffracts from the $\chi^{(2)}$ grating via the processes of nonlinear Bragg diffraction and nonlinear Raman–Nath diffraction. Great efforts have been devoted to understanding these nonlinear diffraction processes [9–12], and further interest is focused on their applications in broadband SHG [4,6], virtual beam generation [13,14], and orbital angular momentum (OAM) modulation [15]. Although it is possible to manipulate the diffraction angle of the nonlinear Raman–Nath SH signals by tuning the operation temperature [10] or the incident angle of the FF beam [11], or employing randomized nonlinear photonic crystals (NPCs) to provide multiple reciprocal lattice vectors (RLVs) [4,6,14], it fails when two or more FF beams are introduced and consequent SH beams need to be controlled simultaneously and separately on purpose.

In this Letter, we propose a scheme for flexibly manipulating the nonlinear Raman–Nath diffraction in an aperiodic nonlinear crystal, and experimentally demonstrate the spatial modulation of the nonlinear Raman–Nath SH signals. Different from the nonlinear Raman–Nath diffraction in periodic gratings, where varying FF leads to distinct angular distribution of SH signals, we succeed in making the SH signals with various wavelengths emit along the same direction by specifically manipulating the $\chi^{(2)}$ nonlinearity of the lithium tantalite crystal. We also discuss how the FF beam waist (BW) and its position of incidence at the engineered grating affect the diffraction emission of the nonlinear Raman–Nath SH signals.

Here, we examined periodically poled lithium tantalite (PPLT) with two different FF beams, 1200 and 1150 nm. This *Z*-cut crystal was set in the schematic arrangement shown in Fig. 1(a). An optical parametric amplifier (OPA) pumped by a regeneratively amplified Ti:sapphire laser was used as the FF source, which delivers 100 fs laser pulses at a repetition rate of 1 kHz. The FF beam was loosely focused onto the crystal, creating a waist radius of approximately 500 μm in the crystal. A CCD camera was used to record the spatial intensity distribution of the SH waves projected on a screen 20 cm behind the crystal. In Fig. 1(b), dashed lines indicate the positions of the SH signals on the screen, red for the 1200 nm FF beam and yellow for the 1150 nm FF beam. It is obvious that shorter wavelengths lead to smaller external angles of SH signals. Since the SH field of the nonlinear Raman–Nath diffraction is determined by the condition

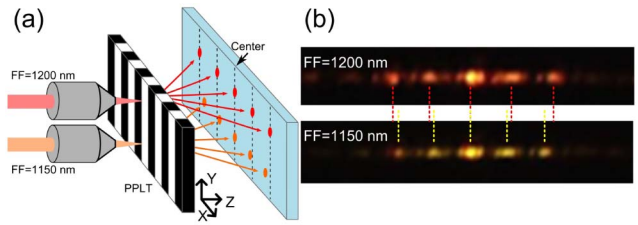

Fig. 1. (a) Schematic arrangement of the nonlinear Raman–Nath SHGs with different FF beams in PPLT. (b) Measured SH signals with various FF beams; when the FF beam alters from 1200 to 1150 nm, the spacing between SH peaks turns narrower.

of momentum conservation in the transverse direction [12], it is difficult to simultaneously and flexibly modulate colorful SH waves on purpose via the nonlinear Raman–Nath diffraction in an NPC with constant poling period.

To solve the problem, we introduced the concept of aperiodic NPCs to facilitate complex diffraction arrangements, which would provide richer and deliberate RLVs [16,17] to satisfy the momentum condition. We began with the amplitude of the SH field via the nonlinear Raman–Nath diffraction, which can be expressed on the assumption of undepleted pump approximation and small-angle approximation as [12]

$$A_2(\kappa_x, z) = -i\beta_2 z e^{iz(\Delta k+\kappa_x^2/2k_2)/2}\mathrm{sinc}[z(\Delta k + \kappa_x^2/2k_2)/2] \times \int g(x)A_1^2(x)e^{i\kappa_x x}\mathrm{d}x, \quad (1)$$

with $\mathrm{sinc}(x) = \sin(x)/x$ and $\mathrm{sinc}(0) = 1$. In Eq. (1), $\beta_2 = k_2\chi^{(2)}/(2n_2^2)$ is the nonlinear coupling coefficient with n_2 being the refractive index at the SH frequency, $\Delta k = k_2 - 2k_1$ is the phase mismatch with k_1 being the FF wave vector and k_2 being the SH wave vector, $g(x)$ is the structure function characterizing the distribution of the second-order nonlinearity $\chi^{(2)}$, κ_x is the RLV of the nonlinear grating along the x direction, and $A_1(x)$ is the amplitude of the fundamental field in the x direction. For the Gaussian beam, $A_1(x) = A_1 e^{(x-x_0)^2/a^2}$, in which A_1, x_0, and a represent the amplitude, central position, and beam width of the fundamental wave, respectively.

Then, we divided the Z-cut lithium tantalite crystal into uniform 10 μm width layers along the x direction, and made some of them poled to change its sign of $\chi^{(2)}$ from positive to negative to modulate the $g(x)$ function. Here, the $g(x)$ function was optimized by the method of the self-adjusting algorithm [18] to realize the same-angle emission for different SH wavelengths, as an example of modulating the nonlinear Raman–Nath diffraction.

Figure 2(a) shows the schematic arrangement of the nonlinear Raman–Nath diffraction with a 1200 nm FF beam in PPLT and APPLT, which was fabricated via standard electric field poling of Z-cut lithium tantalite at room temperature. The period of the PPLT was 20 μm to make sure that each layer was also 10 μm wide. Figure 2(b) indicates the external angles of the SH signals in PPLT (black) and APPLT (red). All SH emissions in PPLT and APPLT were normalized to the signals at 2.78° in PPLT for convenience. Compared with the results in PPLT, a series of new SH peaks in APPLT sprang out with

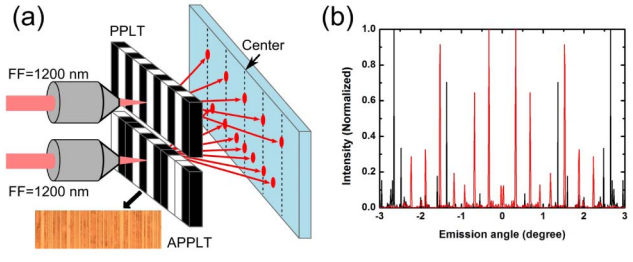

Fig. 2. (a) Schematic arrangements of the Raman–Nath diffraction in PPLT and engineered APPLT. (b) External angles of the Raman–Nath SH signals in PPLT (black line) and engineered APPLT (red line).

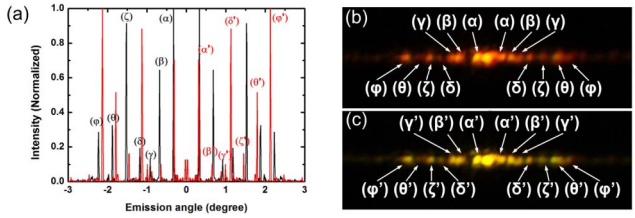

Fig. 3. (a) Calculated angular distribution of the Raman–Nath SH signal in engineered APPLT; black line for the 1200 nm FF beam and red for the 1150 nm FF beam. (b) Experimental image of the Raman–Nath SH signals in engineered APPLT with 1200 nm FF beam and (c) with 1150 nm FF beam.

their strength becoming comparable with those in PPLT. These new generated peaks provide feasibility to satisfy the demand of same-angle emission for different SH wavelengths.

Numerical prediction and experimental evidence is shown in Figs. 3(a)–3(c), where the first-order nonlinear Raman–Nath SH signals with different FF beams—black line for 1200 nm and red line for 1150 nm—emitted at the same angle of α or α'. For the SH spots that are too close that they overlaps each other due to small emission angles, we take the screen far away from the sample such that the SH spots near the center are clearly resolved. And for the sake of briefness, we indexed the SHG by small Greek letters. Table 1 summarizes the predicted and measured external angles of SH signals for both FF beams. The measured and calculated external diffraction angles are in good agreement. Shorter FF wavelengths lead to smaller external diffraction angles, which accords with the results shown in Fig. 1(b) in PPLT. And the demand of same-angle emission for SHG is realized at the angle of α (α'). Thus, it can be confirmed that the nonlinear Raman–Nath diffraction is well manipulated to meet the specific purpose by the engineered $\chi^{(2)}$ grating.

Besides, we make a study of the effect of the FF BW and its position of incidence at the crystal on the nonlinear Raman–Nath diffraction patterns to help better understand the mechanism of nonlinear Raman–Nath diffraction for further SHG manipulation.

Figure 4(a) shows how the SH emission distribution changes along with various FF BWs when the FF beam is focused at the middle of the crystal ($x_0 = 0.5$ L, where L is the length of the crystal). Although a larger FF BW covers more poling layers, the SH emission angles are constant. The only change is the shape of these peaks. For a larger FF BW, the SH peaks are sharper, and for a smaller FF BW, they are broadened and strengthened.

Table 1. SHG with Respective Emission Angles

	FF = 1200 nm		FF = 1150 nm		
SHG	Measured	Calculated	Measured	Calculated	SHG
α	0.24°	0.27°	0.25°	0.27°	α'
β	0.71°	0.69°	0.68°	0.67°	β'
γ	0.93°	0.93°	0.85°	0.89°	γ'
δ	1.23°	1.20°	1.18°	1.12°	δ'
ζ	1.60°	1.53°	1.39°	1.44°	ζ'
θ	1.87°	1.91°	1.82°	1.79°	θ'
ϕ	2.31°	2.27°	2.21°	2.15°	ϕ'

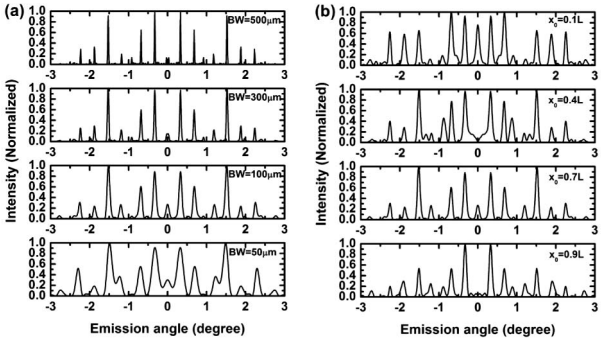

Fig. 4. (a) Effect of FF BW and (b) its position of incidence on the nonlinear Raman–Nath diffraction patterns. In (a), SHG efficiency and bandwidth both increase as the FF BW decreases from 500 to 50 μm; in (b), SH peaks locate at constant directions as the FF beam is focused at different positions (from 0.1 to 0.9 L), but their intensity distributions differ.

We think this is because a wider FF BW covers more space and consequently reduces the uncertainty in the transverse momentum component of the nonlinear grating.

When the FF BW is fixed at a certain value, for instance, 100 μm, the position where the FF beam locates at the crystal will be a more important factor affecting SHG emissions. In Fig. 4(b), the FF beam of 1200 nm is focused at different positions of the designed crystal, from 0.1 to 0.9 L, while their SH emission angles are constant. Although the position of FF beam incidence will not affect the SH emission angles, it deeply influences he relative intensity of each SH peak.

Thus, we can say that the external angles of the nonlinear Raman–Nath SH signals depend on the whole modulation of the $\chi^{(2)}$ grating, not local ones, while the relative intensity of these SH signals is concerned with the FF BW and beam location.

In summary, we succeeded in using a manipulated $\chi^{(2)}$ grating to spatially modulate nonlinear Raman–Nath diffraction. The SH emission distribution is well controlled to present a distinct feature from the case of periodic gratings. As an example of this spatial modulation, the SH signals are made to emit at the same angle with different FF wavelengths, which cannot be achieved in periodic gratings. The experimental results agree well with our numerical calculations, so this manipulation method can be expanded to various applications where diffraction angle controlling is useful. In order to better understand Raman–Nath diffraction modulation, we also study the effect of the FF BW and its incident position on the diffracted SH pattern, and find that nonlinear Raman–Nath diffraction is a whole nonlinear structure-dependent effect, and that SH emission angles are constant no matter how the FF BW or its incident position changes. This work should be useful to modulate the nonlinear Raman–Nath diffraction in various applications such as frequency doubling and ultrashort pulse characterizing. Moreover, twisting the aperiodic superlattice of NPCs will realize various topological charges of the NPCs and a consequent generation of multiple vortices at desired diffraction angles via Raman–Nath diffraction. These multiple vortices with various OAMs could give rise to new applications in microparticle manipulation and multidimensional entanglement generation of photons.

This work is supported by the National Natural Science Foundation of China (Grant Nos. 11174204, 61205110, and 61125503), the National Basic Research Program "973" of China (Grant No. 2011CB808101), and the Foundation for Development of Science and Technology of Shanghai (Grant No. 11XD1402600). We also acknowledge support of crystal fabrication from the National Laboratory of Solid State Microstructures, Nanjing University.

References

1. S. Zhu, Y. Zhu, Y. Qin, H. Wang, C. Ge, and N. Ming, Phys. Rev. Lett. **78**, 2752 (1997).
2. R. T. Bratfalean, A. C. Peacock, N. G. R. Broderick, K. Gallo, and R. Lewen, Opt. Lett. **30**, 424 (2005).
3. M. Gong, Y. Chen, F. Lu, and X. Chen, Opt. Lett. **35**, 2672 (2010).
4. J. Zhang, Y. Chen, F. Lu, and X. Chen, Opt. Express **16**, 6957 (2008).
5. L. H. Peng, C. C. Hsu, and Y. C. Shih, Appl. Phys. Lett. **83**, 3447 (2003).
6. Y. Sheng, J. Dou, B. Ma, B. Cheng, and D. Zhang, Appl. Phys. Lett. **91**, 011101 (2007).
7. K. Gallo, M. Levenius, F. Laurell, and V. Pasiskevicius, Appl. Phys. Lett. **98**, 161113 (2011).
8. A. Shapira and A. Arie, Opt. Lett. **36**, 1933 (2011).
9. A. Arie, N. Habshoosh, and A. Bahabad, Opt. Quantum Electron. **39**, 361 (2007).
10. Y. Sheng, J. Dou, B. Ma, B. Cheng, and D. Zhang, Appl. Phys. Lett. **91**, 101109 (2007).
11. S. M. Saltiel, D. N. Neshev, W. Krolikowski, A. Arie, O. Bang, and Y. S. Kivshar, Opt. Lett. **34**, 848 (2009).
12. Y. Sheng, Q. Kong, W. Wang, K. Kalinowski, and W. Krolikowski, J. Phys. B **45**, 055401 (2012).
13. S. M. Saltiel, D. N. Neshev, W. Krolikowski, N. Voloch-Bloch, A. Arie, O. Bang, and Y. S. Kivshar, Phys. Rev. Lett. **104**, 083902 (2010).
14. A. S. Aleksandrovsky, A. M. Vyunishev, A. I. Zaitsev, A. A. Ikonnikov, and G. I. Pospelov, Appl. Phys. Lett. **98**, 061104 (2011).
15. N. Voloch Bloch, K. Shemer, A. Shapira, R. Shiloh, I. Juwiler, and A. Arie, Phys. Rev. Lett. **108**, 233902 (2012).
16. S. Zhu, Y. Zhu, and N. Ming, Science **278**, 843 (1997).
17. R. Lifshitz, A. Arie, and A. Bahabad, Phys. Rev. Lett. **95**, 133901 (2005).
18. M. Lu and X. Chen, J. Nonlinear Opt. Phys. Mater. **16**, 185 (2007).